1
The Physics and Modeling of Biofunctionalized Nanoelectromechanical Systems

Mark R. Paul and Jerry E. Solomon

1.1
Introduction

Experimental fabrication and measurement are rapidly approaching the nanoscale (see, e.g. Refs. [1–4]). With this comes the potential for many important discoveries in both the physical and life sciences, with particularly intense attention in the fields of medicine and biology [5]. As Richard Feynman famously predicted in the early 1960s, there is indeed plenty of room at the bottom [6, 7]. A particularly promising avenue of research with the potential to make significant contributions is that involving what we will call biofunctionalized nanoelectromechanical systems [(BIO)NEMS]. This is a large and burgeoning field, and we do not attempt to present a survey, but rather we have picked an interesting example of a (BIO)NEMS device in order to highlight the dominant physics and types of modeling issues that arise.

This is not to imply that molecular-scale science is something new – scientists and engineers have been manipulating atoms and molecules for decades. (For an interesting discussion about where nanotechnology fits in with molecular science, see Ref. [8].) However, one new and exciting feature is the ability to fabricate micro- and nanoscale structures that can be used to manipulate, interact and sense biological systems at the single-molecule level.

For a better perspective of the length scales in question it is useful to place micro- and nanometers on biological scales; a human hair has a diameter of about 1 mm, a red blood cell has a diameter of about 10 μm ($1\ \mu m = 1 \times 10^{-6}$ m), the diameter of the bacteria *Escherichia coli* is about 1 μm, the diameter of the protein lysozyme is about 5 nm ($1\ nm = 1 \times 10^{-9}$ m) and the diameter of a single hydrogen atom is about 0.1 nm. When viewed in this context, a device with a characteristic length scale of 100 nm falls in the middle of these biological length scales, i.e. the device is quite large compared to single atoms, yet quite small when compared to single cells or large molecules. It is important to consider this when modeling these systems, as we illustrate below.

The force landscape descriptive of biological and chemical interactions occurs at the piconewton scale ($1\ pN = 10^{-12}$ N). Biologically relevant force magnitudes are

Nanotechnologies for the Life Sciences Vol. 4
Nanodevices for the Life Sciences. Edited by Challa S. S. R. Kumar

ISBN: 3-527-31384-2

related to the breaking and manipulation of chemical bonds. For example it takes hundreds of piconewtons to break covalent bonds, and on the order of 10 pN to break a hydrogen bond or to describe the entropic elasticity of a polymer (see, e.g. Refs. [9, 10]).

The dominant biological time scales of small numbers of molecules are also dictated by their chemical interactions. The time scales of chemical reactions vary over many orders of magnitude, e.g. protein conformational changes can take of the order of milliseconds, binding reactions such as those that occur between transcription factors and genes or between enzymes and substrates are of the order of seconds, covalent bond modifications such that occur with phosphorylation is of the order of minutes, and new protein synthesis in a cell can take tens of minutes.

With these biological length, force and time scales in mind it becomes clear that a major challenge facing the successful development of a single-molecule biosensor is to measure on the order of tens of piconewtons on microsecond time scales. Despite the rapid advancement of new technologies such as surface plasmon resonance [11], optical tweezers [12, 13], microneedles [14, 15] and scanning force microscopy [16–19], detailed knowledge of the real-time dynamics of biomolecular interactions remains a current challenge.

An attractive device with the potential to measure the biophysical properties of a single molecule is based upon the dynamics of nanoscale cantilevers in fluid. In discussing the physics and modeling of (BIO)NEMS we will focus on this type of device. In some aspects this device can be thought of as the miniaturization of atomic force microscopy (AFM) which depends upon the response of micron-scale cantilevers. The invention of AFM [20] has revolutionized surface science, paving the way for direct measurements of intermolecular forces and topographical mapping with atomic precision for a wide array of materials, including semiconductors, polymers, carbon nanotubes and (CNTs) biological cells (see Refs. [21, 22] for current reviews). AFM is most commonly performed in one of three different driven modalities; contact mode, noncontact mode and tapping mode. In contact mode, the cantilever remains in contact with the surface and direct measurements are made based upon the cantilever response as it interacts with the sample. Despite its great success, contact-mode microscopy raises concerns about strong adhesive forces, friction and the damage of soft materials. In response to these issues emerged the noncontact- and tapping-mode modalities which are often referred to as dynamic AFM [23–28].

In noncontact mode, an oscillating cantilever never actually makes impact with the surface, yet its response alters due to an interaction between the cantilever tip and surface forces. The noncontact mode allows the measurement of electric, magnetic and atomic forces. In tapping mode, the cantilever oscillates near the sample surface making very short intermittent contact. Commonly the oscillation amplitude is held fixed through a feedback loop and as the cantilever moves over topographical features of the sample, the change in deflection is measured and related to the surface features. As a result of this minimal impact, and by greatly reducing the effects of adhesion and friction, the tapping mode has become the method of

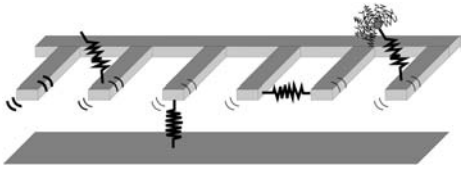

Figure 1.1. Schematic illustrating possible single-molecule detection modalities using small-scale cantilevers immersed in fluid.

choice for high-resolution topographical measurements of soft and fragile materials that are difficult to examine otherwise.

We would like to focus here upon something quite different – the stochastic dynamics of a passive cantilever in fluid. By passive we mean that the cantilever is not being dragged along a surface or forced to tap a surface, but that the cantilever is simply immersed in the fluid. However, recall that at microscopic length scales there is a sea of random thermal molecular noise. Experimental measurement is often limited by this inherent thermal noise; however, with current technology this noise can be exploited to make extremely sensitive experimental measurements [29] including the highly sensitive measurements to be made by gravitational wave detectors [30].

The basic idea is illustrated in Fig. 1.1. A small cantilever placed in fluid will exhibit stochastic dynamics due to the continual buffeting by water molecules that are in constant thermal motion (Brownian motion). In Fig. 1.1, all of the cantilevers will exhibit such oscillations; the four dark lines around each cantilever tip are meant to indicate these oscillations and their degree of shading represents the relative magnitude of these oscillations. One way to measure such oscillations in the laboratory would be through the use of optical methods. The cantilever on the far left is bare and is simply a reference cantilever placed in fluid. The adjacent cantilevers suggest various detection modalities that could also be considered. The fundamental idea is that in the presence of a biomolecule, either attached directly to a single cantilever or between the a cantilever and something else, the cantilever response will change. Measuring this change can then be used to detect the presence of a single biomolecule or, in more prescribed situations, details of the response will yield information about the dynamics of the molecule being probed.

An important advantage of this approach is that small cantilevers have large resonant frequencies, allowing the measurement of these dynamics on natural chemical time scales. In fact, nanoscale cantilevers immersed in water can have resonant frequencies in the megahertz range. The last cantilever on the right shows the case where the target biomolecule is bound between the cantilever and a very large molecule. The purpose of this would be to take advantage of its large surface area and, as a result, its increased fluid drag to enhance the change in response.

An additional complication is that the stochastic dynamics of cantilevers placed in an array, such as those shown in Fig. 1.1, will become coupled to one another through the resulting fluid motion. In other words, if one cantilever moves this

will cause the fluid to move, which will cause the adjacent cantilevers to move and *vice versa*. At first this may appear as just another component of background noise to contend with. However, it is interesting to point out that this correlated noise can be exploited to significantly increase the sensitivity of these measurements. Consider measuring the cross-correlation of the fluctuations between two cantilevers in fluid supporting a tethered biomolecule. By examining only the correlated motion of the two cantilevers we have effectively eliminated the random uncorrelated component of the noise acting on each cantilever. In fact, this approach has been used to measure femtonewton forces (1 fN $= 10^{-15}$ N) on millisecond time scales between two micron-scale beads placed in water [12]. Additionally, this approach was used to quantify the Brownian fluctuations of an extended piece of DNA tethered between the beads leading to the resolution of some long-standing issues concerning the dynamics of single biomolecules in solution [13].

Whatever the manner in which the measurements will actually be made in the laboratory, it will be essential to have a firm understanding of the complex and sometimes counterintuitive physics at work on the these scales in order to interpret them (for an excellent introduction to the modeling of micro- and nanoscale systems, see Ref. [31]).

The purpose of this chapter is to shed some light upon this for the particularly illustrative case where the Brownian noise of small cantilevers in fluid is exploited for potential use as a single-molecule biosensor. Before these measurements can be made and understood, the following questions must be answered:

(a) What are the stochastic dynamics of an array of nanoscale cantilevers immersed in fluid in the absence of the target biomolecules?
(b) How much analyte will arrive at the sensor and what are the time scales for its capture?
(c) Successful measurements will require the discernment between the noise when the biomolecule is attached and the background noise. What signal processing schemes can be used to make these measurements?

We address these questions in the following sections.

1.2 The Stochastic Dynamics of Micro- and Nanoscale Oscillators in Fluid

1.2.1 Fluid Dynamics at Small Scales

The dynamics of fluid motion at small scales contains many surprises when compared with what we are accustomed to in the macroscopic world. In fact most of life involves the interactions of small objects in fluidic environments (see Ref. [32] for an introduction or Refs. [33, 34] for a detailed discussion).

At the molecular scale a fluid is clearly composed of individual molecules. How-

ever, most fluid analysis is done assuming that the fluid is a *continuum*. What this implies is that at any particular point in space (no matter how small) the properties of the fluid (velocity, pressure, etc.) are well defined and well behaved. Another way to think of this is that for any experimental measurement in question we assume that our probe is effectively sampling the average behavior of many molecules.

As our domain of interest becomes smaller it is clear that this assumption will eventually break down. This raises the difficult question – at which point does the continuum approximation become invalid? An approximate answer can be provided by physical reasoning. In the continuum limit one would like the mean free path of collisions of the fluid molecules to be much smaller that a characteristic fluid length scale. This idea is captured by the Knudsen number $\mathrm{Kn} = \lambda/L$, where λ is the mean free path and L is a characteristic length scale. For the case of water, and of liquids in general, the molecules are always in very close contact with one another and the characteristic mean free path can be approximated by the diameter of a single molecule. For water this yields $\lambda \approx 0.3$ nm.

For the stochastic oscillations of small cantilevers we will use the cantilever half-width $w/2$ as the characteristic length. This is because while a cantilever oscillates most of the fluid flows around spanwise over the cantilever. Assuming the cantilever has a width of $w = 1$ μm and is immersed in water yields $\mathrm{Kn} \approx 6 \times 10^{-4}$. Since $\mathrm{Kn} \ll 1$ this indicates that the continuum approximation is good for the fluid dynamics even at these small scales. A quantitative understanding of when the continuum approximation breaks down and what the effects will be is currently an active and exciting area of research with many open questions (see, e.g. Ref. [35]).

The classical equations of fluid dynamics in the continuum limit are the well-known Navier–Stokes equations (see Ref. [36] for a thorough treatment):

$$R_\omega \frac{\partial \vec{u}}{\partial t} + R_u \vec{u} \cdot \vec{\nabla} \vec{u} = -\vec{\nabla} p + \nabla^2 \vec{u}, \tag{1}$$

$$\vec{\nabla} \cdot \vec{u} = 0 \tag{2}$$

Equation (1) is an expression of the conservation of momentum (we have neglected the body force due to gravity). Equation (2) expresses the conservation of mass for an incompressible fluid. We have written the equations in nondimensional form using L, U and T as characteristic length, velocity and time scales, respectively. Two nondimensional parameters R_ω and R_u emerge in Eq. (1) that multiply the two inertial terms on the left-hand side.

It is worthwhile discussing these two parameters in more detail, which will lend some insight into the dominant physics at small scales in fluids. The parameter:

$$R_u = \frac{UL}{\nu_f} \tag{3}$$

expresses the ratio between convective inertial forces and viscous forces (where ν_f is the kinematic viscosity of the fluid, for water $\nu_f \approx 1 \times 10^{-6}$ m^2 s^{-1}). This is the

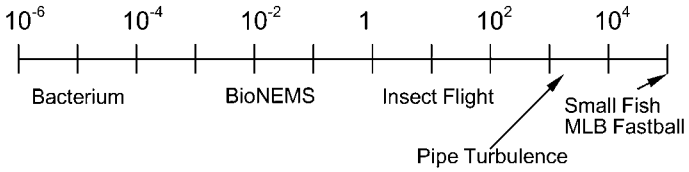

Figure 1.2. Examples of different phenomena occurring over a range of 10 orders of magnitude in the velocity-based Reynolds number, R_u.

velocity-based Reynolds number. It is clear that for micron or nanoscale devices both the characteristic velocity and length scales become quite small, resulting in what is commonly referred to as the low Reynolds number regime. A precise definition of what is meant by ''low'' is not clear. For perspective, Fig. 1.2 illustrates the Reynolds numbers for some particular cases of interest. Note the vast range of phenomena that occurs over 10 orders in magnitude of the Reynolds number. As the Reynolds number decreases, the effects of viscosity dominate inertial effects. For example, if a 1-μm microorganism swimming in water at 10 μm s^{-1} suddenly turns off its source of thrust, say by flagellar or cilia motion, it will come to rest in the fraction of an angstrom. This is nothing like what we are used to on the macroscale. An important consequence when $R_u \ll 1$ is that the nonlinear convective inertial term $\vec{u} \cdot \vec{\nabla}\vec{u}$ becomes negligible. As a result, the equations become linear, greatly simplifying the analysis. The parameter:

$$R_\omega = \frac{L^2}{\nu_f T} \tag{4}$$

expresses the ratio between inertial acceleration forces and viscous forces. Notice that if we take the characteristic velocity to be simply L/T, the frequency and the velocity-based Reynolds numbers become equivalent. However, it is useful not to make this assumption here because we want to consider further the case where the oscillations are imposed externally and the inverse frequency of these oscillations is taken as the time scale. The result is the frequency-based Reynolds number,

$$R_\omega = \frac{\omega w^2}{4\nu_f} \tag{5}$$

where again we have used the cantilever half-width, $w/2$, as the characteristic length scale.

The frequency-based Reynolds is the appropriate Reynolds number to describe micro- or nanoscale cantilevers immersed in fluid. Let us consider further the type of cantilever currently under consideration for the next generation of biosen-

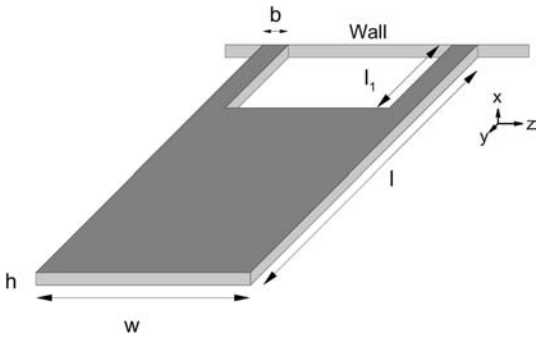

Figure 1.3. Schematic of a proposed cantilever geometry for use as a single-molecule biosensor (not drawn to scale): $l = 3$ μm, $w = 100$ nm, $l_1 = 0.6$ μm, $b = 33$ nm. The cantilever is silicon with a density $\rho_s = 2330$ kg m^{-3}, Young's modulus $E_s = 125$ GPa and spring constant, $k = 8.7$ mN m^{-1} [2, 41].

sors. Approximate values for the cantilever geometry are a width $w \approx 1$ μm, height $h \approx 100$ nm, resonant frequency $\omega \approx 2\pi \times 1$ MHz and we will assume water is the working fluid. As we show later, the maximum cantilever deflection due to Brownian motion will be of the order of $0.01h$ (and often much less depending upon the particular geometry in question). Using these numbers the characteristic velocity is $U = 0.01h\omega$, which yields a velocity-based Reynolds number of $R_u = 3 \times 10^{-3}$. Since $R_u \ll 1$, the nonlinear inertial term can be neglected. However, the frequency-based Reynolds number is $R_\omega = 1.6$. As a result, the first inertial term must be kept in Eq. (1), making the resulting linear analysis more difficult. The governing equations are now:

$$R_\omega \frac{\partial \vec{u}}{\partial t} = -\vec{\nabla} p + \nabla^2 \vec{u} \tag{6}$$

$$\vec{\nabla} \cdot \vec{u} = 0 \tag{7}$$

These equations are known as the time-dependent Stokes equations. In what follows we will drop the subscript ω on R_ω and assume that R represents the frequency-based Reynolds number. Although these equations are linear it is still a formidable challenge to derive an analytical solution for all but the simplest scenarios. One such example is when the cantilever is modeled as an oscillating two-dimensional (2-D) cylinder (discussed in more detail in Section 1.2.3). However, even in simple cases the fluid-coupled motion of arrays of oscillating objects still presents a challenge. This is in addition to the fact that most experimental geometries are not simple, which further complicates the analysis (e.g., see Fig. 1.3). This has led to the development of an experimentally accurate numerical approach to calculate the stochastic dynamics of small-scale cantilevers [37] (discussed below).

1.2.2
An Exact Approach to Determine the Stochastic Dynamics of Arrays of Cantilevers of Arbitrary Geometry in Fluid

At first sight the determination of the stochastic dynamics of an array of fluid-coupled nanoscale oscillators appears quite challenging. Considering the nature of the equations (a system of coupled partial differential equations) and the complex geometries under consideration for experiments, the appeal of a numerical solution is apparent. However, the important question then arises of how to carry out such a numerical investigation? One approach that may come to mind is to perform stochastic simulations of the precise geometries in question that resolves the Brownian motion of the fluid particles as well as the motion of the cantilevers. In principle, this could be done in the context of a molecular dynamics simulation. However, this would be extremely difficult, if possible at all. Two major problems with this approach are:

(a) There are simply too many molecules. A small box with side length of $L = 10$ μm will contain of the order of 10^{13} water molecules. For low Reynolds number flows fluid disturbances are long range and will be of the order of microns even if the oscillators are nanoscale. The length scale of the fluid disturbance scales as approximately $\sqrt{\nu_f/\omega}$. This length scale describes the distance from the oscillating cylinder over which the bulk of the fluid momentum is able to diffuse.
(b) There are vastly disparate time scales. For every oscillation of the cantilever, many water collisions will have had to occur. On average, a water molecule undergoes a collision every picosecond ($1\ \text{ps} = 1 \times 10^{-12}$ s). However, the cantilever oscillates about once per microsecond. In other words, a million water molecules collide with the cantilever for every single cantilever oscillation – imposing considerable overhead upon our numerical scheme. To make matters worse, in order to get good statistics the numerical solution will have to run for many cantilever oscillations or, equivalently, many numerical simulations will have to be run for different initial conditions and averaged.

However, there is a much better approach if one exploits the fact that the system is in *thermodynamic equilibrium*. This allows the use of powerful ideas from statistical mechanics and, in particular, the fluctuation–dissipation theorem, which relates equilibrium fluctuations with the way a system, that has been slightly perturbed out of equilibrium, returns to equilibrium. In other words, if one understands how a systems dissipates near equilibrium, one understands how that same system fluctuates at equilibrium. The fluctuation–dissipation theorem was originally discussed by Callen and Greene [38, 39]; also see Chandler [40] for an accessible introduction.

It has recently been shown that the fluctuation–dissipation theorem allows for the calculation of the stochastic equilibrium fluctuations of small-scale oscillators using only standard *deterministic* numerical methods [37]. For the case of small

cantilevers in fluid, the dissipation is mostly due to the viscous fluid altough internal elastic dissipation of the cantilever could be included if desired.

We will introduce the use of this approach for the case of two opposing cantilevers as shown in Fig. 1.7(a). Consider one dynamic variable to be the displacement of the cantilever on the left $x_1(t)$. This is a classical system, so $x_1(t)$ will be a function of the microscopic phase space variables consisting of $3N$ coordinates and conjugate momenta of the cantilever, where N is the number of particles in the cantilever. We now take the system to a prescribed excursion from equilibrium and observe how the system returns to equilibrium, which, in effect, quantifies the dissipation in the system. A particularly convenient way to accomplish this is to consider the situation where a force $f(t)$ has been applied to the cantilever on the left at some time in the distant past and is removed at time zero. The step force is represented by:

$$f(t) = \begin{cases} F_1 & \text{for } t < 0 \\ 0 & \text{for } t \geq 0 \end{cases} \tag{8}$$

This force couples to $x_1(t)$ causing a deflection in the cantilever. For this case the Hamiltonian of the system H is given by:

$$H = H_0 - fx_1 \tag{9}$$

We only consider the case of small f so the response of $x_1(t)$ remains in the linear regime. In the linear response regime, the change in the average value of a second dynamical quantity $X_2(t)$ (here we will use the displacement of the cantilever on the right, which is again a function of the $3N$ coordinates and conjugate momenta) from its equilibrium value in the absence of f is given by:

$$\Delta X_2(t) = \frac{F_1}{k_B T} \langle \delta x_1(0) \delta x_2(t) \rangle_0 \tag{10}$$

where k_B is Boltzmann's constant ($k_B = 1.38 \times 10^{-23}$ J K^{-1}) and T is the absolute temperature. The equilibrium fluctuations are given by:

$$\delta x_1 = x_1 - \langle x_1 \rangle_0 \tag{11}$$

$$\delta x_2 = x_2 - \langle x_2 \rangle_0 \tag{12}$$

where the average $\langle\ \rangle_0$ denotes the equilibrium average in the absence of the force f. However, for our case the cantilevers fluctuate about an equilibrium of zero deflection, $\langle x_1 \rangle_0 = \langle x_1 \rangle_0 = 0$, which then implies that $\delta x_1 = x_1$ and $\delta x_2 = x_2$. The average behavior of the cantilever deflection in the linear response regime is:

$$\Delta X_2(t) = X_2(t) - \langle x_2(t) \rangle_0 \tag{13}$$

However, as just mentioned, $\langle x_2(t)\rangle_0 = 0$, which also implies $\Delta X_2(t) = X_2(t)$ and yields:

$$X_2(t) = \frac{F_1}{k_B T}\langle x_1(0)x_2(t)\rangle_0 \tag{14}$$

Using this result we can calculate a general equilibrium cross-correlation function in terms of the linear response as:

$$\langle x_1(0)x_2(t)\rangle_0 = \frac{k_B T}{F_1} X_2(t) \tag{15}$$

Similarly, the autocorrelation of the fluctuations is given by:

$$\langle x_1(0)x_1(t)\rangle_0 = \frac{k_B T}{F_1} X_1(t) \tag{16}$$

where $X_1(t)$ is the average behavior of the deflection of the cantilever in which the force was applied. The spectral properties of the correlations can be found by taking the cosine Fourier transform of the auto- and cross-correlation functions. This yields the noise spectra, $G_{11}(\nu)$ and $G_{12}(\nu)$, given by:

$$G_{11}(\nu) = \int_0^\infty \langle x_1(0)x_1(t)\rangle \cos(\omega t)\, dt, \tag{17}$$

$$G_{12}(\nu) = \int_0^\infty \langle x_1(0)x_2(t)\rangle \cos(\omega t)\, dt \tag{18}$$

where ν is the frequency defined by $\omega = 2\pi\nu$. The noise spectra are important because they are precisely what would be measured in an experiment.

This result is exact with the only assumptions being classical mechanics and linear behavior. Equations (15) and (16) are extremely useful in that they relate the *stochastic* cantilever dynamics on the left-hand side to its *deterministic* response to the removal of a step force on the right-hand side. In other words, Eq. (16) relates the equilibrium fluctuations of the cantilever to its average deflection as it returns to equilibrium from a prescribed excursion to a nonequilibrium state.

With this in mind, the remaining challenge is to calculate the deterministic quantities $X_1(t)$ and $X_2(t)$ for use in Eqs. (15) and (16). Since the dynamic variables of interest are macroscopic (after all they are the cantilever deflections X_1 and X_2), they can be calculated using the deterministic macroscopic equations which govern the fluid and solid dynamics. This can be from analytics, simplified models or large-scale numerical simulation.

To summarize, the scheme consists of the following steps in a deterministic calculation:

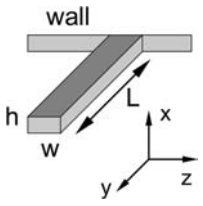

Figure 1.4. Schematic of a simple cantilevered beam of length L, width w and height h.

(a) Apply an appropriate force f that is constant in time and small enough so that the response remains linear. An appropriate force is one that couples to the variable of interest X_1. After applying the force, allow the system to come to steady state.
(b) Turn off the force at a time labeled $t = 0$.
(c) Measure some dynamical variable $X_2(t)$ (which might be the same as X_1 to yield an autocorrelation function) to yield the correlation function of the equilibrium fluctuations via Eqs. (15) and (16).

For the case of small cantilevers in fluid, the fluid motion can be calculated using the incompressible Navier–Stokes equations and the dynamics of the solid structures can be computed from the standard equations of elasticity. Using the sophisticated numerical tools developed for such calculations it is possible to find accurate results for realistic experimental geometries that may be quite complex, e.g. the triangular cantilever design often used in commercial AFM or the paddle geometries currently under investigation for use as detectors of single biomolecules as shown in Fig. 1.3.

1.2.3
An Approximate Model for Long and Slender Cantilevers in Fluid

Let us first consider a long and slender cantilever ($L \gg w, h$) that is fixed at its base and free at its tip with the simple beam geometry as shown in Fig. 1.4. This configuration is particularly useful because this geometry is commonly used for AFM. A simplified and effective model analysis is available for this case [42, 43]. In this model, the dynamics of the beam motion is described using classical elasticity theory:

$$\mu \frac{\partial^2 w(y,t)}{\partial t^2} + EI \frac{\partial^4 w(y,t)}{\partial y^4} = F_f(y,t) \tag{19}$$

where $w(y,t)$ is the displacement of the beam as a function of distance y along the length of the beam and time t, μ is the mass per unit length of the cantilever, E is Young's modulus, I is the moment of inertia of the cantilever, and F_f is the force acting on the cantilever due to the fluid. In this expression we have neglected internal dissipation in the elastic body, tensile forces leading to a stressed or strained

state when the cantilever is at equilibrium and gravity forces (it is straightforward to show that small cantilevers do not bend significantly in a gravitational field). It is important to note that Eq. (19) is coupled with the fluid equations Eqs. (6) and (7) through the force F_f, and that the coupled system of equations are linear. The equations governing beam dynamics are well studied and well understood (see Ref. [44] for an excellent reference on the theory of elasticity). The viscous dissipation in a low Reynolds number fluid is quite large and will dominate any other modes of dissipation such as internal elastic dissipation in the beam itself.

This leaves the important question of how to determine the flow field. Since the beam is long and slender, most of the fluid will interact with the beam by flowing around the sides as opposed to flowing over the beam tip. In this case one can assume that the cantilever is infinite in length and consider only the flow over a 2-D cross-section of the beam [42]. It can then be shown that it is a small correction to then assume that the usually rectangular cross-section of the beam is cylindrical. This is particularly convenient because an analytical solution for the flow field over an oscillating cylinder is available. In fact, the fluid problem was fist solved in 1851 by Stokes; however, for a modern treatment, see Ref. [45].

Since the fluidic damping dominates the cantilever motion we can further simplify the analysis by considering only the fundamental mode of the beam dynamics (the higher harmonics will be damped out by the fluid). This additional simplification aids in clarifying the approach without significantly affecting the results (for the analysis using the full beam equation, see Ref. [42]). The equation of motion describing the fundamental mode of a beam immersed in fluid then becomes:

$$m_e\ddot{\boldsymbol{x}} + kx = F_f + F_B \tag{20}$$

where x represents the deflection of the cantilever tip, m_e is the effective mass of the beam in vacuum, k is the effective spring constant of the beam and F_B is the random force due to Brownian motion. Notice that F_f contains both the fluid damping as well as the fluid loading due to the additional fluid mass that the beam "carries" as it moves.

It is convenient to transform into frequency space by taking the Fourier transform of this equation to give:

$$(-m_e\omega^2 + k)\hat{\boldsymbol{x}} = \hat{F}_f + \hat{F}_B \tag{21}$$

where:

$$\hat{F}_f = m_{cyl,e}\omega^2\Gamma(\omega)\hat{\boldsymbol{x}} \tag{22}$$

and:

$$m_{cyl,e} = 0.243m_{cyl} = 0.243\rho_l\left(\frac{\pi}{4}w^2L\right) \tag{23}$$

which is the effective mass of a fluid cylinder of radius $w/2$, where ρ_l is the fluid density. The prefactor of 0.243 ensures that mode-shape mass is equivalent for the mass of the cantilever, the fluid loaded mass and the fluid damping. The Fourier transform convention we are using is:

$$\hat{\boldsymbol{x}}(\omega) = \int_{-\infty}^{\infty} x(t) e^{-i\omega t}\, dt \tag{24}$$

$$x(t) = \frac{1}{2\pi}\int_{-\infty}^{\infty} \hat{\boldsymbol{x}}(\omega) e^{i\omega t} \tag{25}$$

Here, $\Gamma(\omega)$ is the hydrodynamic function and is defined to be:

$$\Gamma(\omega) = 1 + \frac{4iK_1(-i\sqrt{iR})}{\sqrt{iR}K_0(-i\sqrt{iR})} \tag{26}$$

where K_1 and K_0 are Bessel functions. Note that by this definition the arguments on the right-hand side are R and not the frequency ω. The cantilever is effectively loaded by the fluid which can be characterized by an effective mass, m_f, larger than m_e that takes into account the fluid mass that is also being moved. The fluid also damps the motion of the cantilever, which can be expressed as an effective damping γ_f. Relations for m_f and γ_f can be found by expanding $\Gamma(\omega)$ into its real and imaginary parts Γ_r and Γ_i in Eq. (21), and rearranging such that:

$$-m_f(\omega)\omega^2\hat{\boldsymbol{x}} - i\omega\gamma_f(\omega)\hat{\boldsymbol{x}} + k\hat{\boldsymbol{x}} = \hat{F}_B \tag{27}$$

to give:

$$m_f = 0.243 m_c(1 + T_0\Gamma_r) \sim \Gamma_r(\omega) \tag{28}$$

$$\gamma_f = 0.243 m_{cyl}\omega\Gamma_i \sim \omega\Gamma_i(\omega) \tag{29}$$

Notice that both the fluid loaded mass of the cantilever and the fluidic damping are functions of frequency. The ratio of the mass of the fluid-loaded cantilever to the effective mass of the cantilever in vacuum, m_e, as a function of frequency is shown in Fig. 1.5. The cantilever has a mass of nearly 20 times the effective value at $R \approx 1$. Over 4 orders of magnitude in frequency the mass changes by a factor of about 200. The fluidic damping is shown in Fig. 1.5. There is a slight frequency dependence, over 4 orders of magnitude in frequency the damping changes by a factor of 7, which is much less than the frequency dependence of the mass loading.

From the fluctuation–dissipation theorem the spectral density of the fluctuating force, $G_{F_B}(\nu)$, can be related to the dissipation due to the fluid and is given by:

$$G_{F_B}(\nu) = 4k_B T m_e T_0 \omega\Gamma_i(\omega) \tag{30}$$

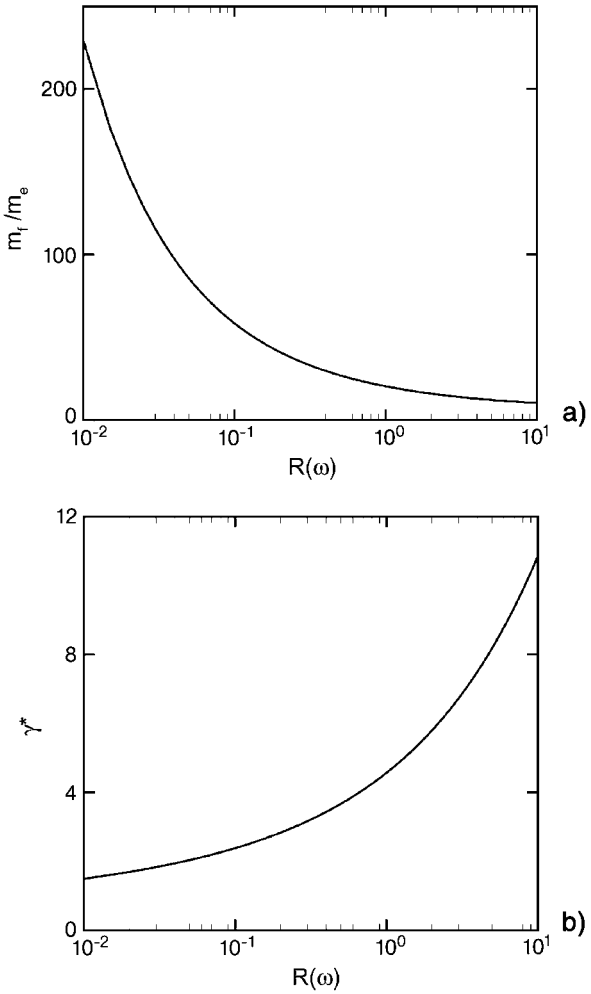

Figure 1.5. (a) The ratio of the mass of a fluid-loaded cantilever to the effective mass of the cantilever in vacuum as a function of the frequency-based Reynolds number. (b) The fluidic damping of a cantilever immersed in fluid as a function of the frequency-based Reynolds number. Shown is the nondimensional damping $\gamma^* = R\Gamma_i(R)$.

where T_0 is the ratio of the mass of fluid contained in a cylindrical volume of radius $w/2$ to the mass of the cantilever. The analysis of Ref. [42] does not take into account the frequency dependence of the damping and assumes that the numerator is constant. Although the frequency dependence of the damping is not large as shown in Fig. 1.5, it should be accounted for. Solving for the spectral density of the displacement fluctuations, $G_x(\nu)$, from Eqs. (21) and (30) yields:

$$G_x(\nu) = \frac{4k_B T}{k}\frac{1}{\omega_0}\frac{\tilde{\omega}T_0\Gamma_i(R_0\tilde{\omega})}{\left[(1-\tilde{\omega}^2(1+T_0\Gamma_r(R_0\tilde{\omega})))^2+(\tilde{\omega}^2T_0\Gamma_i(R_0\tilde{\omega}))^2\right]}$$

where $\tilde{\omega} = \omega/\omega_0$ is the frequency relative to the vacuum resonance frequency $\omega_0 = \sqrt{k/m}$ and R_0 is the frequency-based Reynolds number using ω_0. Using the equipartition of energy theorem and applying it to the cantilever's potential energy, we arrive at:

$$\frac{1}{2}k\langle x^2\rangle = \frac{1}{2}k_B T \tag{31}$$

Using this we scale $G_x(\nu)$ in Eq. (31) such that:

$$\int_0^\infty |\hat{\boldsymbol{x}}(\omega)|^2\,d\omega = \frac{k_B T}{k} \tag{32}$$

The value of ω at the maximum value of $|\hat{\boldsymbol{x}}(\omega)|^2$ yields a theoretical prediction of the fundamental frequency in fluid ω_f. Once ω_f is known, an approximation for the quality factor of the oscillator, Q, is:

$$Q \approx \frac{\frac{1}{T_0}+\Gamma_r(\omega)}{\Gamma_i(\omega)} \tag{33}$$

Equation (33) is valid only for $Q \gtrsim 1/2$ because it neglects to account for the frequency dependence of the mass and fluid loading in Eq. (27) (by considering only the explicit frequency dependence) which become very important for highly overdamped cantilevers (i.e. $R \lesssim 1$).

Using what we have discussed so far let us quantify the stochastic dynamics of an AFM placed in water. We consider a cantilever with the simple beam geometry as shown in Fig. 1.4. The cantilever dimensions are length $L = 197$ μm, width $w = 29$ μm and height $h = 2$ μm. These are chosen so that we can compare with the analytical and experimental results of Ref. [43]. From beam theory, the effective spring constant of a cantilever is:

$$k = \frac{3EI}{L^3} \tag{34}$$

which, for the cantilever in question, yields $k = 1.3$ μN m^{-1}. Using the approach described in Section 1.2 we use a step force $F_1 = 26$ nN and calculate the deterministic response of the cantilever, $X_1(t)$, as it returns to equilibrium. For detailed information on the particular computation algorithm we used to solve the deterministic fluid–solid equations, see Refs. [46, 47]. The value of $\langle x_1(0)x_1(0)\rangle^{1/2}$ is interesting in that it yields the magnitude of the deflections that would be expected

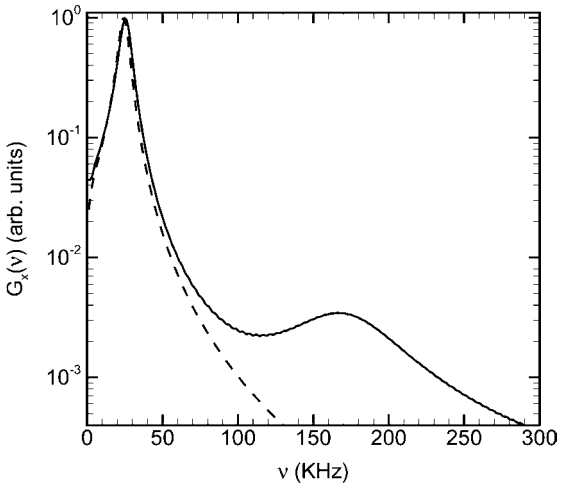

Figure 1.6. The noise spectrum as calculated from full finite element deterministic numerical simulation (solid line) and the noise spectrum from the approximate analytical theory (dashed line) for an AFM immersed in water (for experimental results see cantilever c2 in Ref. [43]). The full numerical simulations include all of the cantilever modes including two that are shown in the frequency range of the figure identified by the two peaks in the simulation results. The analytical model only considers the fundamental mode of the cantilever oscillation resulting in only one peak. Note that more modes could be included if desired; however, as shown in the figures, the higher-frequency modes are strongly damped and will not be significant in experiment. The micron-scale cantilever used for this calculation is of the geometry shown in Fig. 1.4, and has a length $l = 197$ μm, width $w = 29$ μm and height $h = 2$ μm. The applied step force is $F_1 = 26$ nN.

in an experiment. For this case we find that $\langle x_1(0)x_1(0)\rangle^{1/2} = 3.16 \times 10^{-21}$ m^2. This indicates that the deflection of the cantilever due to Brownian motion in an experiment is about 0.056 nm or about 0.003% of the thickness of the cantilever – an extremely small value even on an atomistic scale. Multiplying this quantity by the spring constant gives an estimate of the force sensitivity of 73.1 pN, which is clearly too large to be used as a biological force detector (recall biological force scales are around 10 pN). The noise spectrum is shown in Fig. 1.6, where there is good agreement with the approximate analytical theory available for this case.

1.2.4
The Stochastic Dynamics of a Fluid-coupled Array of (BIO)NEMS Cantilevers

We now use this approach to find the auto- and cross-correlation functions for the equilibrium fluctuations in the displacements of the tips of two nanoscale cantilevers with the experimentally realistic geometries depicted in Fig. 1.3. For this case we would like to emphasize that no analytical expressions or simplified models are currently available. However, we can again use full numerical simulations and exploit the fluctuation theorem, which remains exact.

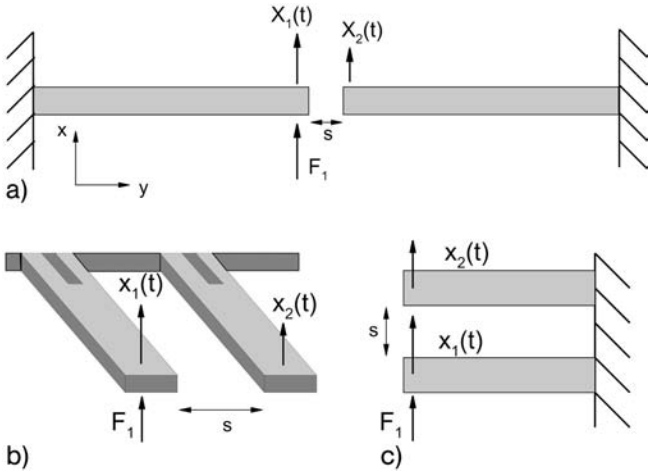

Figure 1.7. Schematic showing various cantilever configurations. In all configurations the step force F_1 is released at $t = 0$, resulting in the cantilever motion referred to by $X_1(t)$. The motion of the neighboring cantilever is $X_2(t)$ and is driven through the response of the fluid. (a) Two cantilevers with ends facing, (b) side-by-side cantilevers and (c) cantilevers separated along the direction of the oscillations.

To do this we again calculate the deterministic response of the displacement of each cantilever tip, which we call $X_1(t)$ and $X_2(t)$ after switching off at $t = 0$ a small force applied to the tip of the first cantilever, F_1, given by Eq. (8). Various possible cantilever configurations are shown in Fig. 1.7(a–c); however, we will only consider the case where two cantilevers face one another end-to-end as shown in Fig. 1.7(c).

Again, the equilibrium auto- and cross-correlation functions for the fluctuations x_1 and x_2 are given by Eqs. (15) and (16), and the noise spectra $G_{11}(\nu)$ and $G_{12}(\nu)$ are given by Eqs. (17) and (18). The cantilever autocorrelation function and the two cantilever cross-correlation function are shown in Fig. 1.8(b and c, respectively). The value of $\langle x_1(0)x_1(0)\rangle$ is 0.471 nm^2, indicating that the deflection of the cantilever due to Brownian motion in an experiment would be 0.686 nm or about 2.3% of the thickness of the cantilever. Multiplying this quantity by the spring constant gives an estimate of the force sensitivity of 6 pN; therefore, a (BIO)NEMS cantilever with this geometry is capable of detecting the breakage of a single hydrogen bond, indicating its potential as a single-molecule biosensor. The cross-correlation of the Brownian fluctuations of two facing cantilevers is small compared with the individual fluctuations. The largest magnitude of the of the cross-correlation is -0.012 nm^2 for $s = h$ and -0.0029 nm^2 for $s = 5h$. The noise spectra for both the one- and two-cantilever fluctuations are shown in Fig. 1.9(a and b).

The variation in the cross-correlation behavior with cantilever separation as shown in Fig. 1.8(c) can be understood as an inertial effect resulting from the nonzero Reynolds number of the fluid flow. The flow around the cantilever can be separated into a long-range potential component that propagates instantaneously in

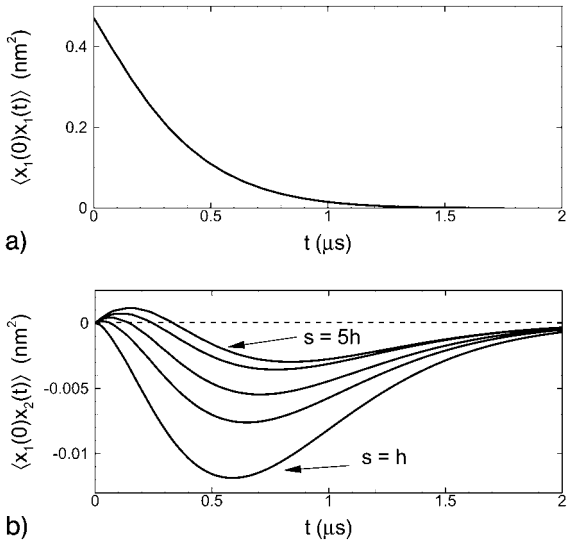

Figure 1.8. Predictions of the auto- and cross-correlation functions of the equilibrium fluctuations in displacement of the cantilevers shown in Figs. 1.3 and 1.7(a). The step force applied to the tip of the first cantilever is $F_1 = 75$ pN. (a) Autocorrelation and (b) cross-correlation of the fluctuations (5 separations are shown for $s = h, 2h, 3h, 4h$ and $5h$, where only $s = h$ and $5h$ are labeled, and the remaining curves lie between these values in sequential order).

the incompressible fluid approximation and a vorticity containing component that propagates diffusively with diffusion constant given by the kinematic viscosity ν_f. For step forcing, it takes a time $\tau_\nu = s^2/\nu_f$ for the vorticity to reach distance s. For small cantilever separations the viscous component dominates, for nearly all times,

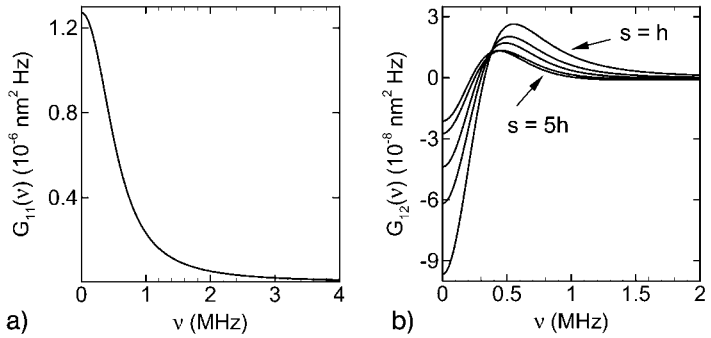

Figure 1.9. (a) The noise spectrum $G_{11}(\nu)$ and (b) the noise spectrum $G_{12}(\nu)$ as a function of cantilever separation s for two adjacent experimentally realistic cantilevers. Five separations are shown for $s = h, 2h, 3h, 4h$ and $5h$, where only $s = h$ and $5h$ are labeled, and the remaining curves lie between these values in sequential order.

and results in the anticorrelated response of the adjacent cantilever in agreement with [12]. However, as s increases, the amount of time where the adjacent cantilever is only subject to the potential flow field increases, resulting in the initial correlated behavior.

The complex fluid interactions between individual cantilevers in an array are still an area of active research. Nevertheless, using the thermodynamic approach described here it is now possible to describe quantitatively, with experimental accuracy, the stochastic dynamics of micro- and nanoscale oscillators in fluid. A compelling feature about these results is that the proposed experiments are just beyond the reach of current technologies, making the theoretical results that much more important, as the insight gained will be critical in guiding future efforts.

1.3 The Physics Describing the Kinetics of Target Analyte Capture on the Oscillator

Now that we have developed the methods necessary to understand the stochastic dynamics of small cantilevers in fluid we turn to the physics describing the capture of target analyte. In order to provide analyte specificity, cantilever surfaces are generally *functionalized* to contain an array of receptor molecules complementary to the target analyte (ligand). This functionalization is carried out by constructing a self-assembling monolayer (SAM), consisting of alkanethiol chains, to which specific receptor molecules are linked. Among other things, the overall performance of (BIO)NEMS cantilever-type sensors will depend on the analyte–receptor capture kinetics and we now discuss a number of issues related to this problem. The basic situation for analyte binding to the functionalized surface of a cantilever is shown in Fig. 1.10.

The binding of analyte from bulk solution to a fixed array of receptors located on a cantilever tip can be described by the kinetic equations relevant to the case of ligand binding to cell surface-bound receptors [48–50], i.e.:

$$\frac{\mathrm{d}B}{\mathrm{d}t} = \left[k_{\mathrm{on}} L_{\mathrm{o}} R_{\mathrm{o}} - (k_{\mathrm{on}} L_{\mathrm{o}} + k_{\mathrm{off}}) B\right] \left[1 + \frac{k_{\mathrm{on}}(R_{\mathrm{o}} - B)}{k_{+}}\right]^{-1} \tag{35}$$

where B is the number of analyte–receptor bound complexes, L_{o} is the analyte concentration and R_{o} is the total number of receptors in the functionalized array. This model equation describes the reversible biochemical reaction:

$$R + L \leftrightharpoons B \tag{36}$$

The parameters k_{on} and k_{off} are the usual forward and reverse rate constants for analyte–receptor binding, and k_{+} is the so-called diffusion rate constant, which for the case at hand is just $k_{+} = 4\pi \mathscr{D} a_{\mathrm{c}}$. The quantity $\mathscr{D}$ is the analyte diffusion coefficient and a_{c} is a length which characterizes the size of the functionalized area,

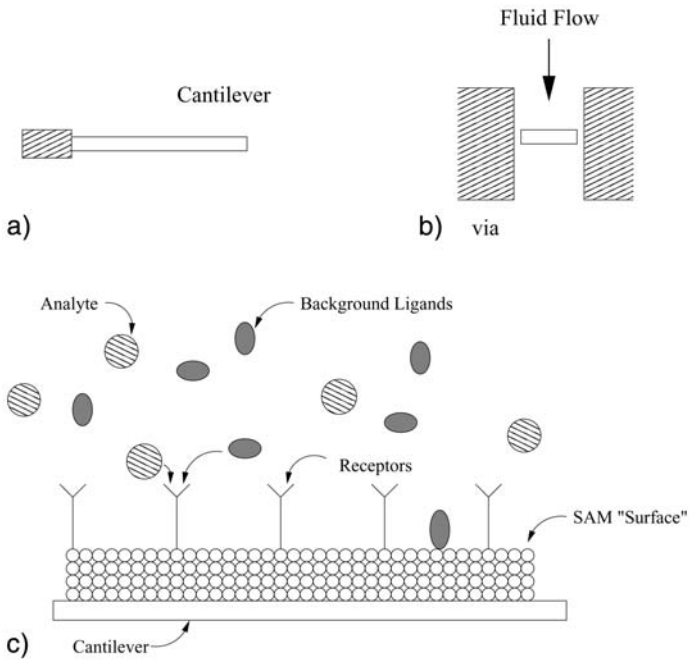

Figure 1.10. (a) The side view of a single cantilever. (b) A schematic placing the cantilever in a via. Fluid flows through the via and around the cantilever shown as a rectangular box in the center. (c) A closeup view of a cantilever tip that has been biofunctionalized.

e.g. its width. Defining new variables, $u = B/R_o$ and $\tau = k_{off}t$, this equation may be put into the more useful nondimensional form:

$$\frac{du}{d\tau} = \frac{K' - (1 + K')u}{[1 + \beta(1 - u)]} \tag{37}$$

with dimensionless parameters $K' = L_o k_{on}/k_{off}$ and $\beta = R_o k_{on}/k_+$. This rather simple kinetic equation describes the analyte–receptor binding under reaction-diffusion conditions, where the parameter β indicates the extent to which the binding is reaction limited ($\beta \ll 1$) or diffusion limited ($\beta \gg 1$).

To give the reader some quantitative insight into this problem, consider the case of biotin–streptavidin ligand–receptor binding. The functionalized region of the cantilever tip is taken to have an area of 1 μm^2, with a total of 10^4 receptors linked to the SAM surface. Note that receptor densities achievable using SAM construction are several orders of magnitude larger than those observed for specific receptors found on biological cell surfaces. The forward binding rate constant is approximately $k_{on} = 5 \times 10^6$ M^{-1} s^{-1}, with a reverse rate constant of $k_{off} \sim 10^{-3}$ s^{-1}. In

addition, we find that $k_+ \approx 10^{12}$ M^{-1} s^{-1}; thus, $\beta = 0.05$ and the ligand–receptor binding process is essentially reaction limited. In fact, for cantilever-type devices designed for detection of biomolecules, we find that the capture process is almost invariably reaction limited. This means that the capture kinetics is dominated by the k_{on} and k_{off} rates of the analyte–receptor pair.

There are two issues of importance when it comes to evaluating the performance of these devices:

(a) The ultimate sensitivity, which will depend on the total number of analytes captured on the cantilever surface;
(b) The time required to achieve a specified sensitivity, which is determined by the capture kinetics.

If no other processes of significance are involved in analyte capture, then ultimate sensitivity can be estimated from a steady-state solution of the model equation given above. Thus, at steady-state, the fraction of total surface receptors that are bound by analyte is given by:

$$u_s = \frac{L_o K_a}{(1 + L_o K_a)} \tag{38}$$

where K_a is the analyte–receptor binding *affinity*. However, depending on the actual analyte–receptor rate constants and the analyte concentration, this may take a considerable time to achieve.

In addition to the basic model equation describing the capture of analyte from bulk solution to surface-bound receptors, there are at least two additional processes that should be considered in connection with sensor performance evaluation:

(a) The effects of background *contaminant* biomolecules;
(b) possible surface-enhanced analyte–receptor binding.

Interference by contaminant biomolecules may arise from two distinct mechanisms. The first of these is by *competitive* binding with the surface receptors, thus lowering the number of receptors available for analyte capture. Competitive binding effects may be analyzed by using a straightforward extension of the basic model equation discussed above. Results of such analyses show that these effects may generally be neglected even for background biomolecule concentrations approaching 10 times the analyte concentration. This is of course largely due to the fact that binding affinities for such biomolecules are 1–3 orders of magnitude smaller than the analyte–receptor binding affinities. The second mechanism involves nonspecific binding of contaminant biomolecules to the SAM surface itself and would be important if analyte detection were accomplished by mass-loading effects. Even though achievable receptor surface densities for these devices approach 10^{12} cm^{-2}, a molecule in solution still ''sees'' mostly bare SAM surface. Thus, contaminant biomolecules may become attached to the cantilever through nonspecific surface

binding. If one treats the alkanethiol end groups as discrete binding sites on the SAM surface, then this problem may be handled by a model equation analogous to the analyte–receptor capture kinetics equation.

Since the concept was first introduced by Adam and Delbruck [51], the possibility of so-called surface-enhanced ligand–receptor binding has been studied by a number of investigators [48, 52, 53]. This mechanism involves a two-step process:

(a) Nonspecific binding of ligand from bulk solution to a surface;
(b) Ligand–receptor binding following 2-D diffusion along the surface.

Although this process may easily be modeled by a pair of coupled kinetic equations, actual quantitative assessment is made difficult by the lack of reliable values for the relevant parameters, i.e. surface nonspecific binding rate and the so-called *collision-coupling* rate constant, k_c [48]. The parameter k_c is the rate constant for a surface-diffusing ligand to bind with a surface-bound receptor and is a difficult quantity to measure experimentally. Nevertheless, it may be useful to attempt to estimate the magnitude of this effect for a particular device implementation since it can result in significant enhancement of the analyte capture efficiency for certain combinations of parameters.

Without considering the parameters of a fully specified sensor it is difficult to give general estimates for cantilever capture performance. However, if we consider the k_{on}, k_{off} rates of the biotin–actin system described above, then the binding affinity will be $K_a = 5 \times 10^9\ \mathrm{M}^{-1}$. Thus, the steady-state receptor coverage is expected to be 33% for an analyte concentration of 0.1 nM. While this represents a very substantial capture efficiency, it should be noted that for these parameter values it will take many 10s of seconds to approach this coverage. This simple example points up an important issue that often arises when attempting to implement specific sensors of this type: One must usually make a trade-off between achievable sensitivity and the time required to make a measurement. A number of applications of these sensors require that detection of the presence of analyte be accomplished in times that are less than 1 s; not infrequently one wishes to achieve millisecond (or less) detection times.

So far the discussion has assumed that analyte transport to the cantilever is accomplished by diffusion only; however, most proposed cantilever sensor implementations involve the use of a microfluidic system to provide constant flow of analyte in a carrier fluid. Thus, in principle, one must consider analyte capture in the context of a reaction–diffusion–convection problem and examine the impact of convection on analyte capture efficiency. Given the previous discussion regarding the reaction rate-limited nature of the analyte capture process, one expects that convection will not have a significant impact on capture efficiency. We can also arrive at this conclusion based on two different fluid dynamics arguments. If one can show that diffusion effects dominate over convection effects in the system, then our previous argument regarding the reaction-limited character of the process still holds and convection cannot contribute significantly to analyte capture. A dimensionless parameter, the Peclet number:

$$\mathrm{Pe} = \frac{LU}{\mathscr{D}} \tag{39}$$

measures the relative importance of convective flow versus diffusive transport; here, L is a characteristic length of the system, U is the flow velocity and $\mathscr{D}$ is the diffusion coefficient. For example, if we take $L = 1$ μm, $U = 10$ μs^{-1}, and $\mathscr{D} = 100$ μm^2 s^{-1}, then we have $\mathrm{Pe} = 0.1$, and diffusion is the dominant transport process. We may also observe that for laminar flow perpendicular to the cantilever surface a diffusion boundary layer of thickness δ is formed. This boundary layer thickness is given approximately by:

$$\delta \approx L(1/\mathrm{Pe})^{1/3} \tag{40}$$

For the parameter values just used this yields a diffusion boundary layer thickness of about 2.2 μm; thus, at this flow rate essentially all analyte transport to the cantilever surface must be by diffusion. Of course one may also consider significantly increasing the fluid flow velocity; however, nanoscale cantilevers can easily be damaged by high flow rates. Even if the flow velocity is not high enough to actually damage a cantilever, it can result in a ''bending bias'' of the cantilever which can interfere with detection of binding events. We should point out, however, that these arguments should be re-examined when considering specific sensor implementations.

The use of mass-action-derived kinetic equations for the purpose of analyzing analyte capture performance is completely adequate for analyte concentrations down to about 0.1–1.0 nM. However, when we consider analyte concentrations in the picomolar (or smaller) range, concentration fluctuations may become important in describing the overall performance of the sensor system. Recall that an analyte concentration of 1 nM corresponds to a molecular density of slightly less that 1 molecule μm^{-3}. In this event one must resort to stochastic methods for describing the reaction–diffusion process of analyte capture. For this case we mention an approach originally developed by Gillespie [54, 55] for ''exact'' stochastic simulation of coupled chemical reactions. Since the approach has been extended by Stundzia and Lumsden [56] to incorporate diffusion effects, the combined algorithm is suitable for providing a stochastic analysis of the analyte capture problem.

The Gillespie approach is based on the fact that at the microscopic level chemical reactions consist of discrete events that may be described by a joint probability density function (PDF). Thus, given a total of $\mu = 1, 2, \ldots, M$ coupled reactions, consisting of a total of $\nu = 1, 2, \ldots, N$ species, the appropriate joint PDF is $P(\mu, \tau)$, where τ is the time interval between reactions. This is simply the joint probability that the μth reaction occurs after a time interval of τ, which may be written as $P(\mu, \tau) = P(\mu)P(\tau)$. Expressions for the individual probabilities are readily derived; these expressions may then be used to implement a rather simple computer algorithm that simulates the evolution of the discrete species concentrations as a function of time, thus yielding the stochastic kinetics for the system. As Gillespie has shown [57], the resulting algorithm is an ''exact'' simulation of the stochastic master equation describing the coupled chemical system.

As mentioned above, as long as analyte concentrations are expected to be in a range where concentration fluctuations are not important, i.e. greater that about 0.1–1.0 nM, then use of the usual mass-action-derived kinetic equations is perfectly satisfactory in estimating the capture kinetics of the sensors considered here. However, since by its nature the mass-action-derived kinetics computes average values, this method cannot give one any insight into the stochastic behavior of the system. While there are no well-defined rules as to when one must consider fluctuations, it is generally true that when the total number of reactant molecules (ligands) in the reaction volume is only of the order of several hundred, then one should begin to suspect that fluctuations may play an important role in the system behavior. In such cases it is advisable to investigate this possibility through the use of a stochastic simulation algorithm such as the one described above.

1.4
Detecting Noise in Noise: Signal-processing Challenges

Although space does not permit a detailed analysis of the various signal-processing methods that may be used in conjunction with (BIO)NEMS cantilever-type sensors, we present a simple analysis of the most basic signal detection method that one might employ. For this analysis we assume a single passive cantilever that utilizes a piezoresistive transducer to sense the fluctuations in the cantilever tip. As discussed before, the term passive simply means that we do not actively drive the cantilever motion in order to provide for a lock-in detector-type processing system. Under these assumptions, and with no analyte bound to the cantilever, the mean-square displacement of the cantilever tip due to fluid fluctuations is given by:

$$\langle x^2(t)\rangle = \frac{4k_B T\gamma_e}{k^2} \tag{41}$$

where k_B is Boltzmann's constant, T is the temperature, γ_e is the effective damping constant for the cantilever and k is the effective spring constant for the cantilever. The mean-square voltage signal into the front end of a signal-processing system is then just:

$$\langle v^2(t)\rangle = |\mathscr{G}\cdot I|^2\langle x^2(t)\rangle \tag{42}$$

with $\mathscr{G}$ being the transducer conversion coefficient and I being the piezoresistive bias current.

We next assume that the presence of bound analyte on the cantilever tip appears as a change in the effective cantilever damping constant, i.e. $\gamma_e \rightarrow \gamma_e^b$. Note that in this situation our ''signal'' appears as a change in the mean-square fluctuations of the cantilever tip. From a signal detection theory standpoint we are attempting to discriminate against the presence of two random voltages, both being Gaussian

distributed but having different variances. Our expressions for the mean-square voltage fluctuations yield a (power) signal-to-noise ratio, $(\mathrm{SNR})_\mathrm{p}$, of:

$$(\mathrm{SNR})_\mathrm{p} = \frac{\gamma_\mathrm{e}^\mathrm{b}}{\gamma_\mathrm{e}} \tag{43}$$

Note that since our expression for the mean-square displacement fluctuations was essentially derived from a fluctuation–dissipation theorem, these expressions are for a system with infinite bandwidth. Our expression for SNR_p may thus be called an *inherent* signal-to-noise ratio for this detection modality. The simplest possible processing of this signal then amounts to sending it through a low-noise root mean square (r.m.s.) detector with threshold. The threshold is set to achieve the desired balance between probability of detection and false-alarm probability (*cf.* Ref. [58]).

Of course, since it is usually required that one achieve the highest possible system sensitivity, more sophisticated signal-processing techniques than the simple r.m.s. detector are usually required. We will mention only two such possibilities:

(a) Passive detection using a *reference* cantilever;
(b) Active detection using a reference cantilever and lock-in (phase) detection.

In the first case we incorporate an additional cantilever, which is *not* functionalized, into the system. One may then use a technique which is analogous to one developed in the early days of radio astronomy. In this implementation one periodically switches between the reference and sensing cantilevers to make what amounts to a phase-detection measurement of the ''signal'' power. The method allows one to eliminate the front-end electronics noise and to make a much better estimate of the no-signal power, thus allowing an improved signal-to-noise ratio. In the second approach we move to an active system where the reference and sensing cantilevers are subjected to periodic deflection forces that are 90° out of phase. This allows one to directly utilize lock-in amplifier (phase detector) technology to achieve significant enhancements to the achievable signal-to-noise ratio. For details on these and other more sophisticated signal-processing approaches to the detection of cantilever sensor signals, the reader is referred to Refs. [58–60].

1.5
Concluding Remarks

The physics and modeling of (BIO)NEMS devices poses many theoretical challenges that must be faced as experiment continues to push measurement to the nanoscale. In this chapter we have just scratched the surface of this exciting new field. In picking one particular example to focus upon it was our intent to leave the reader with an idea of some of the physics and modeling issues that one may encounter.

Acknowledgments

Our research in the modeling of MEMS and NEMS has benefited from many fruitful discussions with the Caltech BioNEMS effort (M. L. Roukes, PI) and we gratefully acknowledge extensive interactions with this team.

References

1 M. B. Viani, T. E. Schäffer, A. Chand. Small cantilevers for force spectroscopy of single molecules. *J. Appl. Phys. 86*, 2258–2262, **1999**.
2 M. L. Roukes. *Nanoelectromechanical Systems.* condmat/0008187, **2000**.
3 C. Bustamante, J. C. Macosko, G. J. L. Wuite. Grabbing the cat by the tail: manipulating molecules one by one. *Nature 1*, 130–136, **2000**.
4 C. Wang, M. Madou. From MEMS to NEMS with carbon. *Biosens. Bioelectron. 20*, 2181–2187, **2005**.
5 C. Zandonella. The tiny toolkit. *Nature 423*, 10–12, **2003**.
6 R. P. Feynman. There is plenty of room at the bottom. *J. Microelectromech. Syst. 1*, 60–66, **1992**.
7 R. P. Feynman. Infinitesimal machinery. *J. Microelectromech. Syst. 2*, 4–14, **1993**.
8 G. M. Whitesides. The 'right' size in nanbiotechnology. *Nat. Biotechnol. 21*, 1161–1165, **2003**.
9 H. Clausen-Schaumann, M. Seitz, R. Krautbauer, H. E. Gaub. Force spectroscopy with single bio-molecules. *Curr. Opin. Chem. Biol. 4*, 524–530, **2000**.
10 M. Doi, S. F. Edwards. *The Theory of Polymer Dynamics (International Series of Monographs on Physics 73)*. Oxford Science Publications, Oxford, **1986**.
11 C. Tassius, C. Moskalenko, P. Minard, M. Desmadril, J. Elezgaray, F. Argoul. Probing the dynamics of a confined enzyme by surface plasmon resonance. *Physica A 342*, 402–409, **2004**.
12 J.-C. Meiners, S. R. Quake. Direct measurement of hydrodynamic cross correlations between two particles in an external potential. *Phys. Rev. Lett. 82*, 2211–2214, **1999**.
13 J.-C. Meiners, S. R. Quake. Femtonewton force spectroscopy of single extended DNA molecules. *Phys. Rev. Lett. 84*, 5014–5017, **2000**.
14 A. Kishino, T. Yanagida. Force measurements by micromanipulation of a single actin filament by glass needles. *Nature 334*, 74–76, **1988**.
15 A. Ishijima, H. Kojima, H. Higuchi, Y. Harada, T. Funatsu, T. Yanagida. Multiple- and single-molecule analysis of the actomyosin motor by nanometer piconewton manipulation with a microneedle: unitary steps and forces. *Biophys. J. 70*, 383–400, **1995**.
16 M. Radmacher, M. Fritz, H. Hansma, P. K. Hansma. Direct observation of enzymatic activity with the atomic force microscope. *Science 265*, 1577–1579, **1994**.
17 N. H. Thomson, M. Fritz, M. Radmacher, J. Cleveland, C. F. Schmidt, P. K. Hansma. Protein tracking and detection of protein motion using atomic force microscopy. *Biophys. J. 70*, 2421–2431, **1996**.
18 M. B. Viani, L. I. Pietrasanta, J. B. Thompson, A. Chand, I. C. Gebeshuber, J. H. Kindt, M. Richter, H. G. Hansma, P. K. Hansma. Probing potein–protein interactions in real time. *Nat. Struct. Biol. 7*, 644–647, **2000**.
19 D. A. Walters, J. P. Cleveland, N. H. Thomson, P. K. Hansma, M. A. Wendman, G. Gurley, V. Elings. Short cantilevers for atomic force microscopy. *Rev. Sci. Instrum. 67*, 3583–3590, **1996**.
20 G. Binnig, C. F. Quate, Ch. Gerber.

Atomic force microscope. *Phys. Rev. Lett. 56*, 930–933, **1986**.

21 F. J. Giessibl. Advances in atomic force microscopy. *Rev. Mod. Phys. 75*, 949–983, **2003**.

22 N. Jalili, K. Laxminarayana. A review of atomic force microscopy imaging systems: applications to molecular metrology and biological sciences. *Mechatronics 14*, 907–945, **2004**.

23 Y. Martin, C. C. Williams, H. K. Wickramasinghe. Atomic force microscope force mapping and profiling on a sub 100-A scale. *J. Appl. Phys. 61*, 4723–4729, **1987**.

24 T. R. Albrecht, P. Grutter, D. Horne, D. Rugar. Frequency-modulation detection using high-Q cantilevers for enhanced force microscope sensitivity. *J. Appl. Phys. 69*, 668–673, **1991**.

25 M. Radmacher, R. W. Tillman, M. Fritz, H. E. Gaub. From molecules to cells: imaging soft samples with the atomic force microscope. *Science 257*, 1900–1905, **1992**.

26 Q. Zhong, D. Inniss, K. Kjoller, V. B. Elings. Fractured polymer/silica fiber surface studied by tapping mode atomic force microscopy. *Surf. Sci. 290*, L688–L692, **1993**.

27 P. K. Hansma, J. P. Cleveland, M. Radmacher, D. A. Walters, P. E. Hillner, M. Benzanilla, M. Fritz, D. Vie, H. G. Hansma, C. B. Prater, J. Massie, L. Fukunage, J. Gurley, V. Elings. Tapping mode atomic force microscopy in liquids. *Appl. Phys. Lett. 64*, 1738–1740, **1994**.

28 R. Garcia, R. Perez. Dynamic atomic force microscopy methods. *Surf. Sci. Rep*. 197–301, **2002**.

29 S. Kos, P. Littlewood. Hear the noise. *Nature 431*, 29, **2004**.

30 Y. Levin. Internal thermal noise in the LIGO test masses: a direct approach. *Phys. Rev. D 57*, 659–663, **1998**.

31 J. A. Pelesko, D. H. Bernstein. *Modeling MEMS and NEMS*. Chapman & Hall/CRC, London, **2003**.

32 E. M. Purcell. Life at low Reynolds number. *Am. J. Phys. 45*, 3–11, **1977**.

33 J. Happel, H. Brenner. *Low Reynolds Number Hydrodynamics*. Springer, Berlin, **1983**.

34 C. Pozrikidis. *Boundary Integral and Singularity Methods for Linearized Viscous Flow*. Cambridge University Press, Cambridge, **1992**.

35 G. Karniadakis, A. Beskok, N. Aluru. *Micro Flows*. Springer, Berlin, **2001**.

36 R. L. Panton. *Incompressible Fluid Flow*. Wiley, New York, **2005**.

37 M. R. Paul, M. C. Cross. Stochastic dynamics of nanoscale mechanical oscillators in a viscous fluid. *Phys. Rev. Lett. 92*, 235501, **2004**.

38 H. B. Callen, T. A. Welton. Irreversibility and generalized noise. *Phys. Rev. 83*, 34–40, **1951**.

39 H. B. Callen, R. F. Greene. On a theorem of irreversible thermodynamics. *Phys. Rev. 86*, 702–710, **1952**.

40 D. Chandler. *Introduction to Modern Statistical Mechanics*. Oxford University Press, Oxford, **1987**.

41 J. Arlett et al. BioNEMS: biofunctionalized nanoelectromechanical systems. To be published.

42 J. E. Sader. Frequency response of cantilever beams immersed in viscous fluids with applications to the atomic force microscope. *J. Appl. Phys. 84*, 64–76, **1998**.

43 J. W. M. Chon, P. Mulvaney, J. Sader. Experimental validation of theoretical models for the frequency response of atomic force microscope cantilever beams immersed in fluids. *J. Appl. Phys. 87*, 3978–3988, **2000**.

44 L. D. Landau, E. M. Lifshitz. *Theory of Elasticity*. Butterworth-Heinemann, London, **1959**.

45 L. Rosenhead. *Laminar Boundary Layers*. Oxford University Press, Oxford, **1963**.

46 H. Q. Yang, V. B. Makhijani. A strongly-coupled pressure-based CFD algorithm for fluid–structure interaction. In: *AIAA-94-0179*, pp. 1–10, **1994**.

47 CFD Research Corp., Huntsville, AL 35805.

48 D. A. Lauffenburger, J. J. Linderman. *Receptors*. Oxford University Press, New York, **1993**.

49 H. C. Berg, E. M. Purcell. Physics of chemoreception. *Biophys. J. 20*, 193–219, **1977**.

50 O. G. Berg, P. H. von Hippel. Diffusion-controlled macromolecular interactions. *Annu. Rev. Biophys. Biophys. Chem. 14*, 131–160, **1985**.

51 G. Adam, M. Delbruck. *Structural Chemistry and Molecular Biology*, A. Rich, N. Davidson (Eds.). Freeman, San Francisco, CA, **1968**.

52 D. Wang, S.-Y. Gou, D. Axelrod. Reaction rate enhancement by surface diffusion of adsorbates. *Biophys. Chem. 43*, 117–137, **1992**.

53 D. Axelrod, M. D. Wang. Reduction-of-dimensionality kinetics at reaction-limited cell surfaces. *Biophys. J. 66*, 588–600, **1994**.

54 D. T. Gillespie. A general method for numerically simulating the stochastic time evolution of coupled chemical reactions. *J. Appl. Phys. 22*, 403–434, **1976**.

55 D. T. Gillespie. Exact stochastic simulation of coupled chemical reactions. *J. Phys. Chem. 81*, 2340–2361, **1977**.

56 A. B. Stundzia, C. J. Lumsden. Stochastic simulation of coupled reaction–diffusion processes. *J. Comp. Phys. 127*, 196–207, **1996**.

57 D. T. Gillespie. Concerning the validity of the stochastic approach to chemical kinetics. *J. Stat. Phys. 16*, 311–318, **1977**.

58 H. L. van Trees. *Detection, Estimation, and Modulation Theory: Part I*. Wiley, New York, **2001**.

59 A. D. Whalen. *Detection of Signals in Noise*. Academic Press, New York, **1971**.

60 J. L. Stensby. *Phase-Locked Loops: Theory and Applications*. CRC Press, Boca Raton, FL, **1997**.